Enabling Technologies toward Fully LTE-Compatible Full-Duplex Radio

Gosan Noh, Hanho Wang, Changyong Shin, Seunghyeon Kim, Youngil Jeon, Hyunchol Shin, Jinup Kim, and Ilgyu Kim

The authors provide technical challenges and solutions for an LTE-compatible full-duplex cellular network, featuring wideband and wide dynamic range support for RF self-interference cancellation and robust and efficient self-interference channel estimation for digital self-interference cancellation. Based on a realistic LTE-based cellular model, their full-duplex radio design is evaluated through system-level simulations and real-world testbed experiments.

ABSTRACT

Full-duplex radio has potential to double spectral efficiency by simultaneously transmitting and receiving signals in the same frequency band, but at the expense of additional hardware and power consumption for self-interference cancellation. Hence, the deployment of a full-duplex cellular network can be realized by employing full-duplex functionality only at an eNodeB, which is supposed to have sufficient computation and power resources, and by scheduling pairs of half-duplex UEs that are in either downlink or uplink. By doing so, fast and smooth full-duplex deployment is possible while minimally affecting the legacy UEs and the rest of the network entities. In this article, we provide technical challenges and solutions for an LTE-compatible full-duplex cellular network, featuring wideband and wide dynamic range support for RF self-interference cancellation, and robust and efficient self-interference channel estimation for digital self-interference cancellation. Based on a realistic LTE-based cellular model, our full-duplex radio design is evaluated through system-level simulations and real-world testbed experiments. Simulation results show that a significant throughput gain can be achieved by the full-duplex technique despite the existence of physical limiting factors such as path loss, fading, and other-cell interference. Testbed measurements reveal that at a bandwidth of 20 MHz, self-interference cancellation up to 37 dB is achieved in the RF domain, and most of the residual self-interference is further cancelled down to the noise floor in the subsequent digital domain.

INTRODUCTION

The explosion of wireless data traffic leads to an exponential increase in the target data rate requirements of the fifth generation (5G) wireless cellular networks. A 5G network is expected to provide 1000-fold capacity gains compared to the existing 4G networks such as 3GPP Long Term Evolution (LTE) and LTE-Advanced (LTE-A) systems [1].

The highly demanding capacity requirements of a 5G network can be met by a combination of increasing cell density, utilizing formerly unused spectrum, and improving spectral efficiency. Among them, full-duplex transmission has recently drawn much attention as a means of potentially doubling spectral efficiency by simultaneously transmitting both the downlink and uplink signals in the same frequency band, which is a prominent advantage compared to the conventional half-duplex schemes such as frequency-division duplex (FDD) and time-division duplex (TDD).

One of the key challenging issues for full-duplex radio is the existence of strong self-interference from the transmit to receiver chains. The self-interference comes from imperfect isolation between the transmit and receive paths and reflections from nearby scatterers. It is usually much stronger than the desired received signal, sometimes even 100 dB or so stronger [2]. Thus, such self-interference should be mitigated before processing the received signals. Otherwise, any information contained in the received signal cannot be properly decoded. In this regard, there have been various attempts to suppress or cancel the self-interference in the RF and digital domains [3–5]. Kim *et al.* presented a point-to-point full-duplex scheme based on polarization-division duplexing [3]. Bharadia *et al.* implemented a full-duplex WiFi radio using analog and digital self-interference cancellation techniques [4]. Huusari *et al.* developed a wideband RF self-interference cancellation circuit having self-adaptive and self-healing features [5].

Different from the above prior works dealing with point-to-point and WiFi links, an attempt to apply full-duplex transmission into a cellular network was recently reported in [6], where the self-interference cancellation for full-duplex transmission is performed only at the eNodeB (i.e., base station) while the user equipments (UEs) are limited to half-duplex transmissions. Combined with an appropriate UE scheduling strategy, this scheme achieves a significant full-duplex gain. Based on this, we further improve the eNodeB-side only full-duplex scheme with the aim of ensuring compatibility with the existing LTE and LTE-A systems. Therefore, we expect a fast and smooth deployment of the full-duplex radio with minimal impact on the legacy UEs and the rest of the network entities.

Hence, in this article, we suggest system architecture and enabling technologies for the full-duplex support in an LTE-compatible cellular network, including:

- Identifying a system description with deployment scenarios and requirements

This work was supported by the Institute for Information & Communications Technology Promotion (IITP) grant funded by the Korea government (MSIP) (No.B0115-16-0001, 5G Communication with a Heterogeneous, Agile Mobile Network in the PyeongChang WInter Olympic Competion.

Digital Object Identifier: 10.1109/MCOM.2017.1600791CM

Gosan Noh, Jinup Kim, and Ilgyu Kim are with the Electronics and Telecommunications Research Institute (ETRI); Hanho Wang is with Sangmyung University; Changyong Shin is with Sun Moon University; Seunghyeon Kim was with Kwangwoon University and now is with GCT Semiconductor Inc.; Youngil Jeon, and Hyunchol Shin are with Kwangwoon University.

0163-6804/17/$25.00 © 2017 IEEE

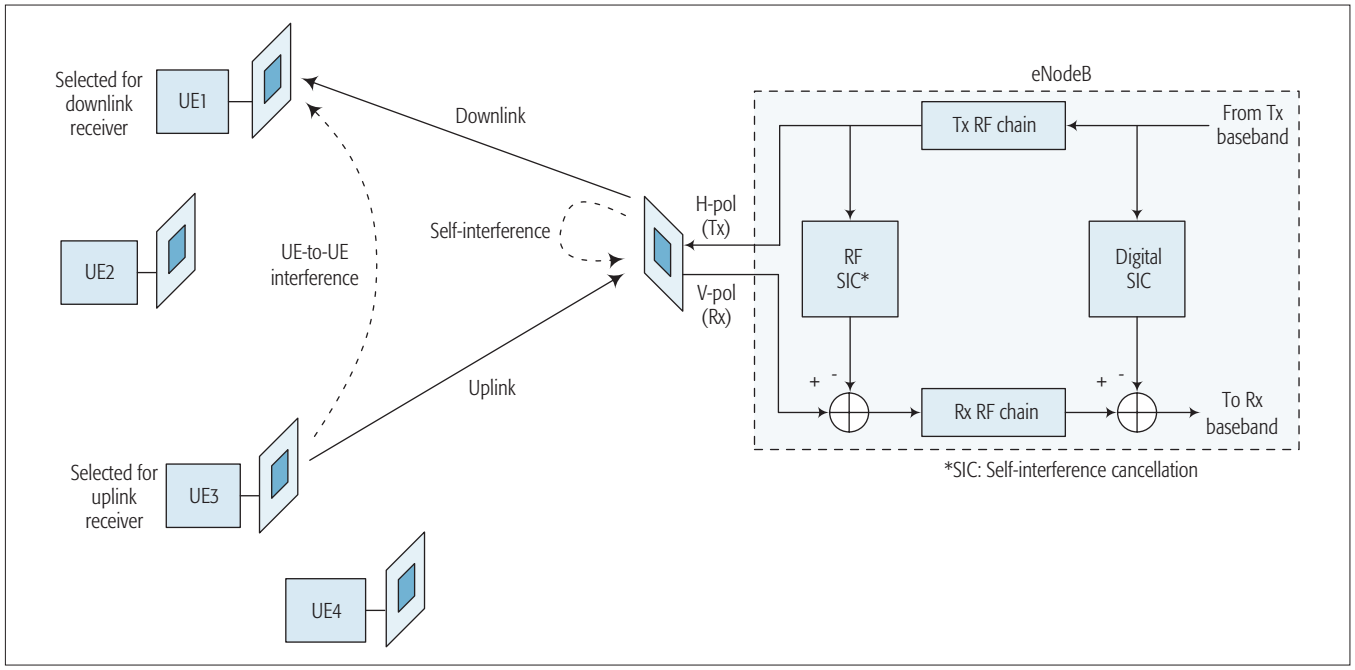

Figure 1. System overview and transceiver structure of the proposed LTE-compatible full-duplex radio.

- Providing some important implementation challenges and solutions focusing on the wideband and wide dynamic range RF self-interference cancellation and the robust and efficient digital self-interference cancellation with special consideration of the compatibility with LTE systems
- Evaluating the system-level performance under the existence of physical factors such as path loss, fading, and other-cell interference
- Describing the LTE-compatible full-duplex testbed and evaluating its real-world performance.

System Description and Requirements

Network Model and Deployment Scenario

We consider a full-duplex cellular system based on the LTE/LTE-A standard where each cell consists of an eNodeB and multiple UEs, as seen in Fig. 1. The full-duplex functionality is implemented only at the eNodeB, while UEs operate in the conventional half-duplex fashion, similar to [6]. The reason for employing full-duplex functionality only at the eNodeB side is twofold. First, UEs tend to have limited hardware and energy resources to support full-duplex operations (e.g., self-interference cancellation in the RF and digital domains). Second, the eNodeB-side-only full duplex facilitates backward compatibility with legacy LTE/LTE-A UEs supporting only either FDD or TDD. As a result, upgrading a half-duplex LTE system into a full-duplex one becomes possible by simply replacing the half-duplex eNodeBs with the full-duplex eNodeBs while not affecting the rest of network entities and interconnections.

Our target deployment scenario is a small cell environment with a low-power eNodeB and low-mobility UEs. With less transmit power (i.e., 20 dB or so less than the macro eNodeB [7]), the required level of self-interference power to be cancelled is considerably scaled down, thereby facilitating the self-interference cancellation with less complexity and less residual interference. The low-mobility properties of UEs ascertain that the self-interference channel remains the same during the self-interference channel estimation and cancellation procedures, allowing reliable self-interference cancellation.

Self-Interference Cancellation

As seen from the right side of Fig. 1, the eNodeB contains several techniques to minimize the self-interference in both analog and digital domains, which include antenna separation, RF-domain cancellation, and digital-domain cancellation. Antenna separation is a technique to physically and/or electrically separate the signal paths between the transmit and receive antennas. One promising candidate is the use of a dual-polarized antenna having two orthogonal polarization components (e.g., transmission in horizontal polarization and reception in vertical polarization) [8, 9]. However, due to imperfect polarization isolation and reflections from nearby scatterers, some self-interference components still remain in the received signal, which need to be further cancelled out using analog RF circuitry and digital signal processing techniques.

RF self-interference cancellation is required to cut down the residual self-interference component in the received RF signal so that after the RF cancellation, the signal level can fall within the dynamic range of the analog-to-digital converter (ADC) in the receiver RF chain. After this, the self-interference component is further cancelled out in the digital domain without the loss due to RF receiver saturation. The RF cancellation capability can be achieved by employing an RF self-interference cancellation circuit that automatically generates a replica signal with the same magnitude but opposite phase with respect to the self-interference component and cancelling it out from the received RF signal.

After the RF cancellation, digital cancellation is performed with the baseband signal in the digital

The RF self-interference cancellation functionality is required to cover a wide channel bandwidth with a wide dynamic range. The bandwidth of the LTE signal ranges from 1.4 MHz to 20 MHz. Thus, the operational bandwidth for the RF self-interference cancellation functionality is expected to cover 20 MHz.

domain after the ADC. Using a priori information on the transmitted signal and the self-interference channel estimate, the digital cancellation can eliminate the self-interference almost to the noise floor by subtracting the generated copy of self-interference from the received baseband signal.

Multiple Access

In order to ensure compatibility, full-duplex operation should be supported in accordance with the existing LTE multiple access schemes, that is, orthogonal frequency-division multiple access (OFDMA) for the downlink and single-carrier frequency-division multiple access (SC-FDMA) for the uplink. Using OFDMA, the data streams intended for different UEs are transmitted on non-overlapping subcarrier sets. Thanks to the orthogonality among the subcarriers, the degradation due to multipath fading can easily be compensated using low-complexity equalization techniques, yielding inter-symbol interference (ISI)- and inter-carrier interference (ICI)-free transmission. One significant drawback of OFDMA is high peak-to-average power ratio (PAPR), degrading the power efficiency of the transmitter. The PAPR can be effectively reduced by adopting SC-FDMA in the uplink where the data symbols are discrete Fourier transform (DFT)-spread before being mapped to the subcarriers. The reason for employing the SC-FDMA only at the uplink is the limited power budget of battery-operated mobile devices. These design objectives for the multiple access are still valid for the full-duplex LTE system. Thus, the transceiver design and signal processing algorithm development for the LTE-compatible full-duplex radio should be done based on OFDMA downlink and SC-FDMA uplink.

Implementation Challenges and Solutions

In order to fulfill the above requirements, some critical technical challenges need to be overcome. Specifically, one of the most challenging issues is self-interference cancellation, which needs to be implemented in both the RF and digital domains while achieving a sufficient level of compatibility with existing LTE systems. Other challenging issues to be addressed in this work are self-interference channel estimation and downlink/uplink synchronization.

RF Self-Interference Cancellation

The RF self-interference cancellation functionality is required to cover a wide channel bandwidth with a wide dynamic range. The bandwidth of the LTE signal ranges from 1.4 to 20 MHz. Thus, the operational bandwidth for the RF self-interference cancellation functionality is expected to cover 20 MHz.

Wide dynamic range capability is needed due to the large fluctuation of the self-interference signal strength. Such fluctuation originates from transmit power variation, channel path loss variation, and isolation level variation between the transmit and receive antennas [10, 11]. The measurement shows that the required dynamic range is greater than a factor of 20 dB [11]. In the following, we discuss how the wideband and wide dynamic range capabilities can be achieved.

Achieving Wideband Self-Interference Cancellation: Wideband channels tend to experience frequency selectivity, that is, the channel response varies with respect to frequency due to the delay spread in the time domain. Exploiting the multicarrier structure of OFDMA, digital self-interference cancellation can overcome this frequency selectivity in the frequency domain by estimating the self-interference channel and cancelling the self-interference signal on a per-subcarrier basis. On the other hand, RF self-interference cancellation has limited ability to perform frequency-dependent operation. Hence, a candidate solution will be employing a multi-tap RF self-interference cancellation circuit that consists of multiple RF self-interference cancellation paths with different time delays [4, 12]. The delay for each path can be adjusted by variable delay lines.

Achieving Wide Dynamic Range Self-Interference Cancellation: Any restriction on the dynamic range of the RF self-interference cancellation circuit limits the ability to adjust the replica signal strength to a level close to the actual self-interference signal remaining at the RF receiver input terminal. If the two power levels do not match, there will remain a significant amount of uncancelled self-interference after the RF self-interference cancellation.

A promising solution to this problem is the employment of a variable-gain amplifier at the replica signal generation path before the cancellation point, as described in detail in our prior work [11]. By adjusting the gain of the variable-gain amplifier according to the fluctuating received self-interference power level, the RF self-interference canceller provides robust and improved cancellation performance.

Self-Interference Channel Estimation

The prerequisite for digital self-interference cancellation is acquiring the accurate information of the self-interference channel. In the LTE/LTE-A systems, reference signals are used for channel estimation: cell-specific reference signals (CRSs) for the downlink and demodulation reference signals (DMRSs) for the uplink. Since we are to perform self-interference cancellation at the eNodeB, the self-interference channel estimation is involved with the CRS.

However, since the current frame structures for LTE and LTE-A were originally designed for the half-duplex modes (i.e., FDD and TDD), the CRS-based self-interference channel estimation is disturbed by the so-called pilot contamination caused by the interference from the simultaneously transmitted uplink resource elements co-located with the CRS, thereby degrading the performance of the digital self-interference cancellation.

In order to tackle the above problem, we employ an uplink nulling technique that prevents a certain portion of uplink resources from being transmitted so that the CRSs for the self-interference channel estimation are not interfered. Although there might be uplink throughput loss due to the uplink nulling, its impact will not be significant considering the traffic asymmetry between the downlink and uplink. The peak data rate requirements of the LTE-A system are 1 Gb/s for the downlink and 500 Mb/s for the uplink, demonstrating significant asymmetry [13]. The

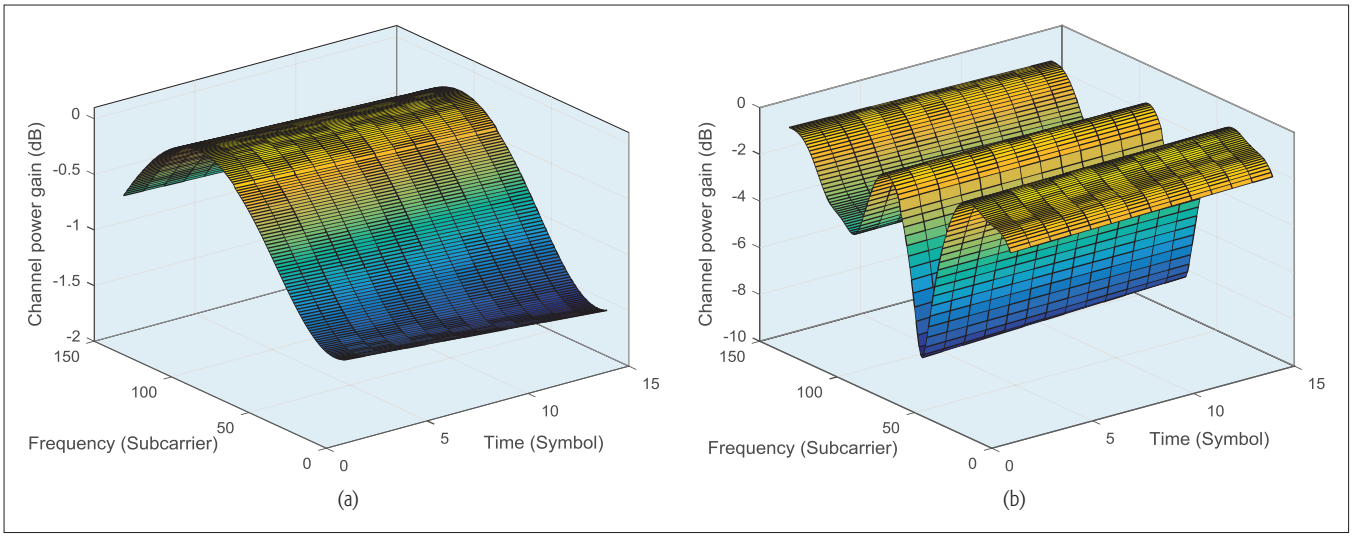

Figure 2. Time-frequency channel responses for slow fading channels: a) EPA 10 MHz; b) EVA 10 MHz.

uplink nulling can be categorized according to the amount and frequency of time-frequency resources to be nulled (i.e., per-subframe/symbol uplink nulling and per-RE uplink nulling).

Per-Subframe/Symbol Uplink Nulling: In slow fading environments with low mobility, the channel gains are supposed to be stable over a timescale that ranges from several orthogonal frequency-division multiplexing (OFDM) symbols to several radio frames. Using Clarke's model, the 50 percent coherence time at the maximum Doppler frequency of 10 Hz is about 42.3 ms [14], which is much larger than the length of a radio frame. This slow fading tendency can be observed in Fig. 2, which shows the simulated time-frequency channel responses for extended pedestrian A (EPA) and extended vehicular A (EVA) models assuming a maximum Doppler frequency of 10 MHz.

Based on the above considerations, as described in Fig. 3a, we can employ a per-subframe nulling scheme that nulls out a designated uplink subframe (i.e., the 0th uplink subframe where the physical broadcast channel (PBCH), the primary synchronization signal (PSS), and the secondary synchronization signal (SSS) are transmitted in the downlink counterpart. By doing so, the self-interference channel estimation can be done within the 0th subframe without interference from the uplink. Then, using the estimated self-interference channel knowledge, the self-interference cancellation is carried out in the rest of the subframes. If the coherence time becomes shorter than a radio frame, per-symbol uplink nulling can be employed where certain symbols (e.g., the first two of 14 symbols in a normal subframe) is nulled out, as seen in Fig. 3b.

The per-subframe/symbol uplink nulling techniques are simple and easy to implement with minimal frame structure changes to the current LTE and LTE-A standards. Only some modification on the uplink scheduler is needed. However, these per-subframe/symbol uplink nulling schemes may suffer from resource waste.

Per-RE Uplink Nulling: In order to solve the above problem, we employ the per-RE uplink nulling where only the uplink REs located at the same

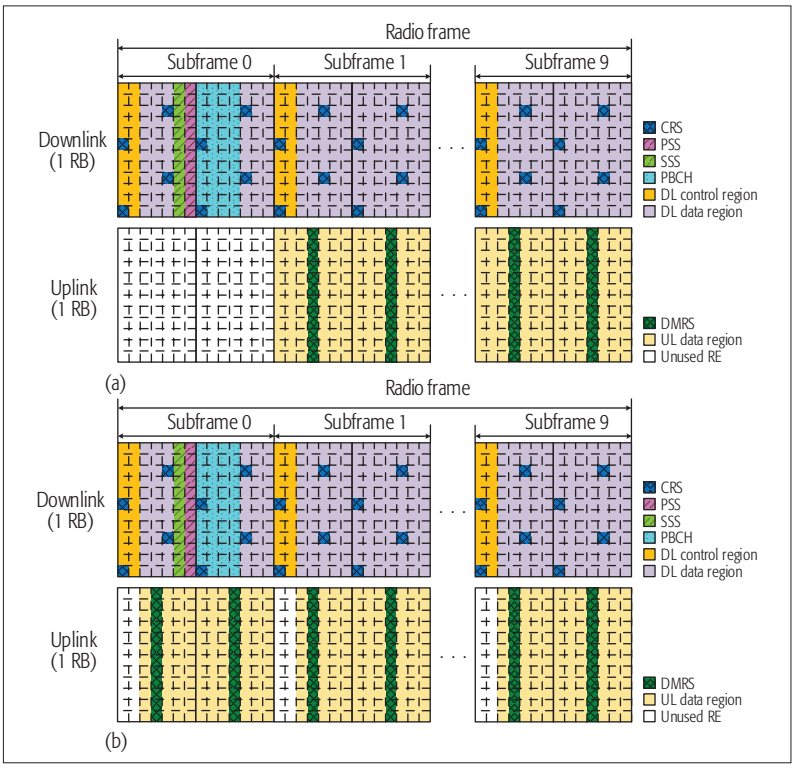

Figure 3. Time-frequency resource grids for per-subframe/symbol uplink nulling; a) per-subframe uplink nulling; b) per-symbol uplink nulling.

time-frequency positions as the downlink CRSs are nulled out. Figure 4a shows an example of per-RE uplink nulling in two consecutive resource blocks. It is clear that with per-RE uplink nulling, the downlink CRSs can be used for self-interference channel estimation without the uplink interference. The resource waste due to the per-RE uplink nulling is only 4.76 percent, which is much lower compared to the full-duplex gain.

The per-RE uplink nulling can be done by allocating the null subcarriers at the subcarrier mapping block of the SC-FDMA transmitter, which can be implemented while causing minimum impact to the LTE/LTE-A standards. At the receiv-

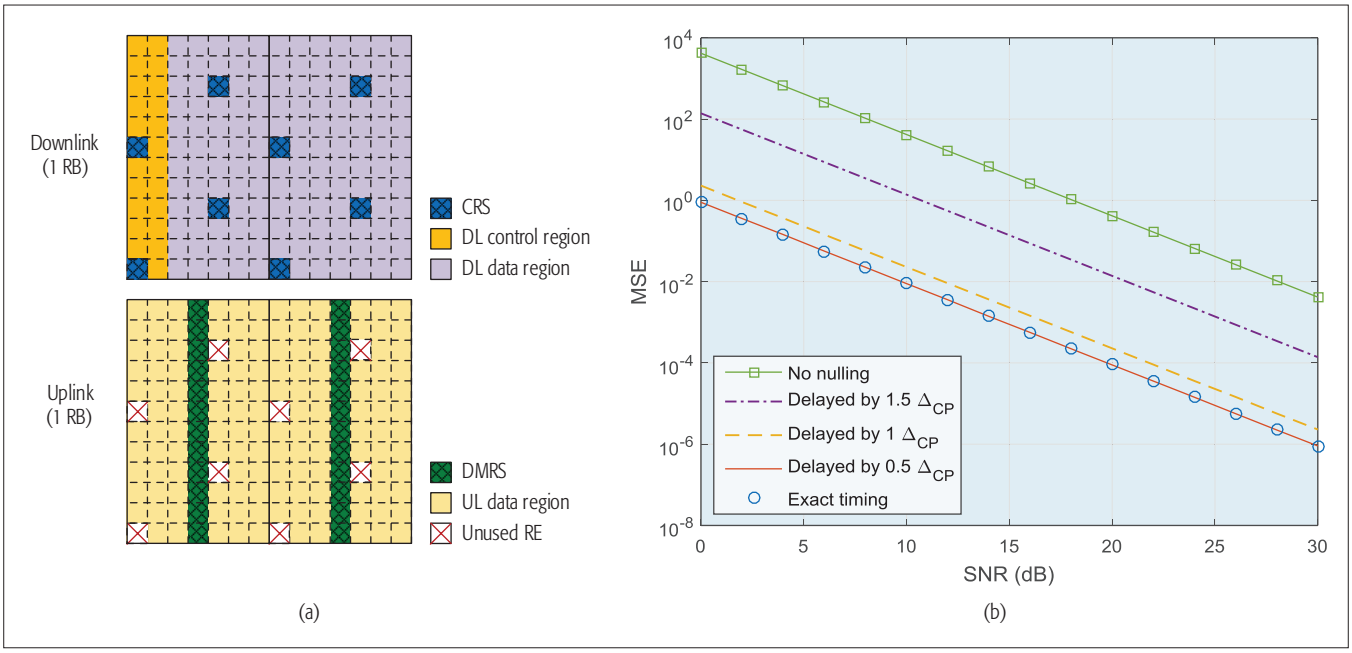

Figure 4. Per-RE uplink nulling: a) time-frequency resource grids for downlink and uplink; b) mean square error vs. interference-to-noise ratio (INR) of the self-interference link.

er, the self-interference channel estimation can be done using the downlink CRSs co-located with the uplink null subcarriers. The self-interference cancellation is then performed, followed by the null subcarrier removal and uplink channel estimation/equalization. In order to ensure backward compatibility, the eNodeB is also required to provide support for legacy UEs that do not support the per-RE uplink nulling by bypassing the null subcarrier removal and self-interference cancellation functionalities.

Frame Synchronization between Downlink and Uplink: The above self-interference channel estimation scheme requires frame synchronization between the downlink and uplink. Without the frame synchronization, the self-interference channel estimation will be disturbed by the interference from the overlapping adjacent uplink symbols. In this regard, uplink timing alignment functionality already present in LTE/LTE-A can be used to align the start time of the received uplink subframe and the transmitted downlink subframe. More specifically, using the timing advance values determined by the network based on the uplink measurement, the UEs carry out timing advance operations. By advancing or delaying the uplink signal, the amount of timing misalignment can be limited to within the cyclic prefix. Once the timing misalignment is less than the cyclic prefix, its effect can easily be overcome by phase compensation in the frequency domain.

The effect of the timing misalignment on the performance of the per-RE uplink nulling-based self-interference channel estimation is shown in Fig. 4b, which depicts the mean square error (MSE) as a function of the interference-to-noise ratio (INR) of the self-interference link. The uplink signal-to-noise ratio (SNR) is assumed to be 20 dB. The curves are plotted for different amounts of the downlink-uplink timing misalignment in terms of the ratio of the cyclic prefix length to the OFDM symbol length Δ_{CP}. As expected, the MSE for the timing misalignment of 0.5 Δ_{CP} is exactly the same as the case with the exact timing. Oppositely, we can see significant MSE degradation for the large timing misalignment case of 1.5 Δ_{CP}. When the timing misalignment is 1 Δ_{CP}, i.e., same as the cyclic prefix length, the MSE is slightly higher than the case of exact timing, which is due to the effect of the delay spread. For comparison, the MSE of the no nulling case is also plotted where the uplink interference is not avoided during the self-interference channel estimation procedure, providing the upper bound.

System-Level Performance Evaluation in an Actual Cellular System

In practical cellular systems, we should consider several physical factors such as distance-dependent path loss, large- and small-scale fading, and other-cell interference in addition to the aforementioned RF and digital impairments. In this regard, we evaluate the system-level performance of the full-duplex-enabled cellular system compared to the conventional half-duplex schemes, FDD and TDD.

System-Level Evaluation Environment: We consider a heterogeneous cellular network where multiple macro and small cells are deployed in the same frequency band. The macro eNodeBs are placed on a hexagonal grid with inter-site distance (ISD) of 500 m. The small eNodeBs and UEs are randomly dropped. The UEs located within the small cell radius of 40 m are connected to the small eNodeB.

Full-duplex functionality is employed at each small eNodeB, which therefore experiences not only the intra-cell interference from itself (i.e., self-interference) but also the inter-cell interference from other macro and small cells. The specific simulation parameters are based on the 3GPP LTE-A outdoor small cell evaluation scenario with co-channel deployment of the macro and small

Parameter	Value
Carrier frequency	2.59 GHz
Bandwidth	20 MHz
Macrocell ISD	500 m
Small cell radius	40 m
eNodeB TX power	Macrocell: 46 dBm Small cell: 30 dBm
UE TX power	27 dBm
Thermal noise density	-174 dBm/Hz
eNodeB noise figure	Macrocell: 5 dB Small cell: 8 dB
UE noise figure	9 dB
Path loss	Macrocell: $128.1 + 37.6\log_{10}(R)$ Small cell: $140.7 + 36.7\log_{10}(R)$
Shadowing std	Macrocell: 8 dB Small cell: 10 dB

(a)

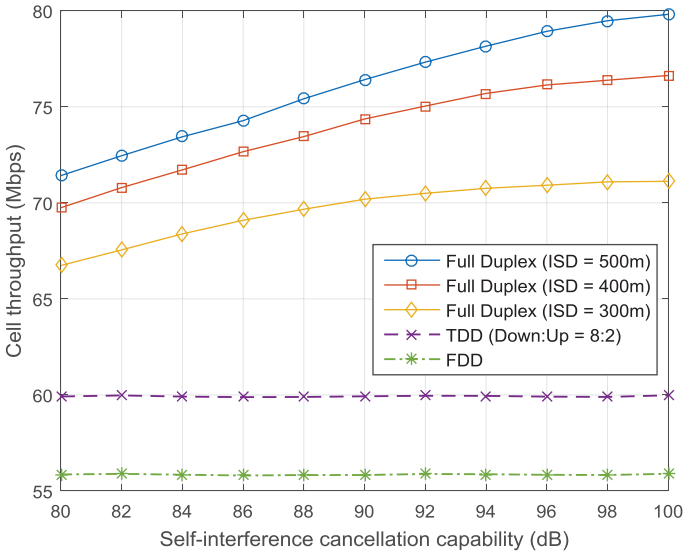

(b)

Figure 5. System-level evaluation results: a) simulation parameters; b) throughput vs. self-interference cancellation capability.

cells [15]. The detailed simulation parameters are described in Fig. 5a.

System-Level Evaluation Results: With the above simulation parameters, we obtained simulation results over different small eNodeB and UE drops, each with 2048 realizations. In Fig. 5b, the average throughput of a UE is plotted, which can be attained through simultaneous downlink and uplink transmissions. Comparisons with the FDD and TDD schemes are also provided. Since the system bandwidth of 20 MHz is assumed for full duplex, 10 MHz bandwidth is employed for each of the DL and UL for FDD. For TDD, DL/UL configuration 2 is employed so that the ratio between the DL and UL is about 80 and 20 percent.

Figure 5b shows that significant throughput gain through the use of full duplex is attainable despite the existence of the real-world physical factors such as path loss, fading, and other-cell interference. The amount of throughput gain is increased with the self-interference cancellation capability (i.e., the total amount of self-interference cancellation using a combination of antenna, RF, and digital cancellations), and is upper-bounded at about 95 dB, which is consistent with the existing literature [6]. The throughput gain of TDD over FDD is due to the fact that the downlink throughput is higher than the uplink throughput.

Testbed Description and Performance Evaluation

In this section, we describe our LTE-based full-duplex testbed in order to evaluate real-world full-duplex performance, especially on both the RF and digital self-interference cancellation capabilities.

Testbed Setup

The testbed for the evaluation of our full-duplex radio design represents the eNodeB side of an LTE-based full-duplex cellular system, which consists of antenna, RF cancellation circuit, and digital cancellation unit, as seen in Fig. 6a.

A dual-polarized microstrip patch antenna is used for the separation between the transmit and receive signal paths. The center frequency is designed to be at 2.59 GHz with the –10 dB bandwidth of 140 MHz. The isolation between the horizontal and vertical ports is measured from –15 dB to –35 dB varying depending on surrounding environmental conditions [11].

The RF cancellation circuit is designed to achieve wide bandwidth and wide dynamic range cancellation capability, as described in [11]. The circuit itself has self-adaptive characteristics to automatically control the amplitude and phase of the replica signal by the use of the vector modulator and the variable-gain amplifier. In order to support wideband cancellation, a two-tap RF cancellation circuit is employed with different delay settings at the input. The delay for each tap is adjusted by using cables with different lengths in this experiment. The optimal cable length difference is found to be 152 cm, which corresponds to a time delay of 7.4 ns after extensive measurements for length difference varying form 0 cm to 200 cm. Wide dynamic range can be supported by the use of a variable-gain amplifier (Avago MGA-638P8). The RF cancellation circuit is powered by ±10 V supply. The local oscillator inputs of the up- and down-conversion mixers are provided by a signal generator at a frequency of 2.59 GHz.

The signal processing for digital cancellation is performed using the NI USRP-2942R software-defined radio (SDR) device that has a Xilinx Kintex-7 field programmable gate array (FPGA) and two independent RF front-ends supporting frequency bands from 400 MHz to 4.4 GHz with the maximum bandwidth of 40 MHz. The SDR is controlled by a host computer using NI LabVIEW Communications Systems Design Suite 1.1 software. The baseband processing functions, including modulation, demodulation, and digital self-interference cancellation, are performed in the FPGA. The transmitter unit generates an LTE-modulated signal, followed by a high-power amplifier that can amplify the transmit signal power level to 20 dBm.

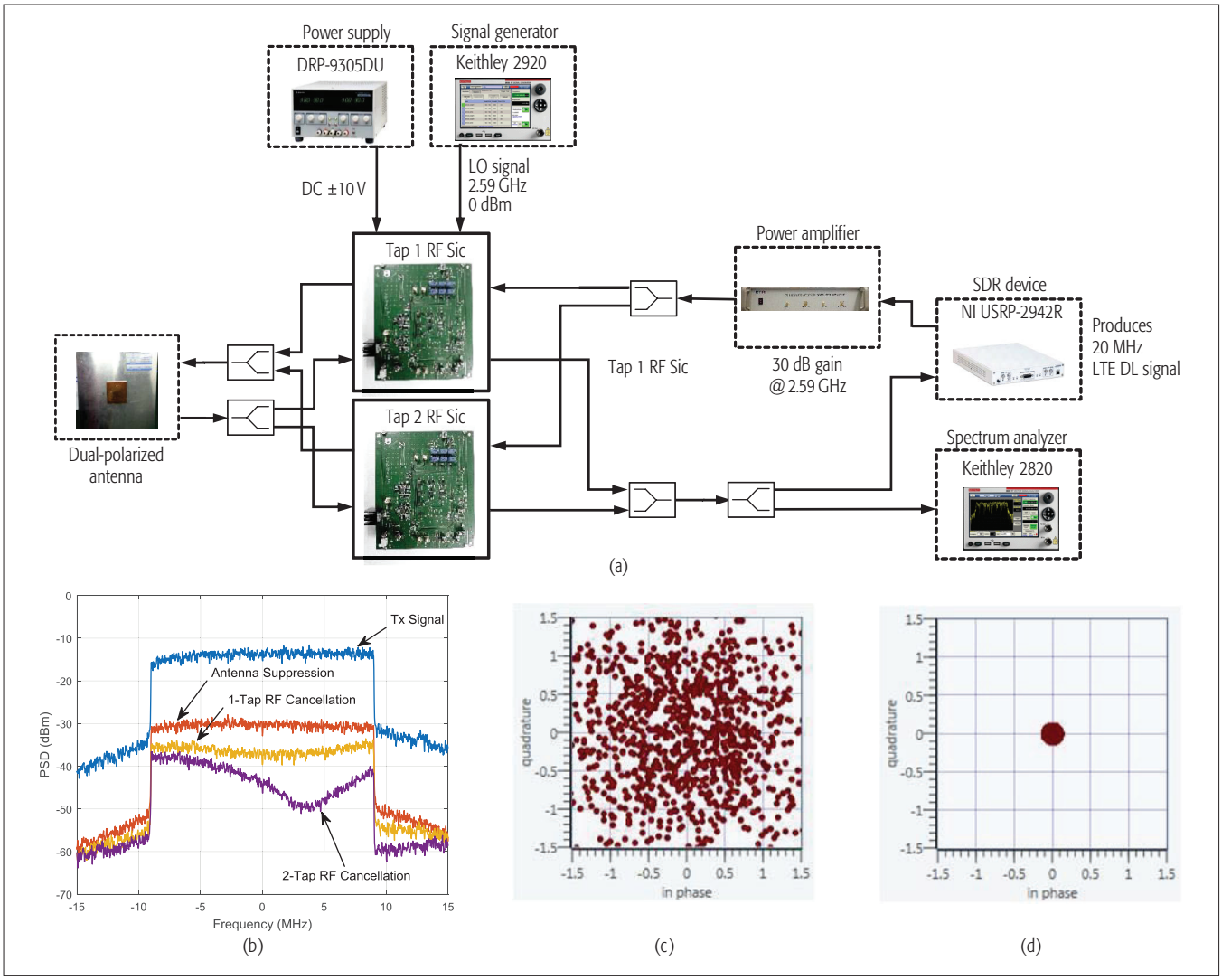

Figure 6. Testbed setup and experimental results: a) testbed setup; b) self-interference cancellation by antenna suppression and RF self-interference cancellation; c) constellation before digital cancellation; d) constellation after digital cancellation.

The implementation of the digital part is based on 3GPP LTE Release 10. The bandwidth is 20 MHz, and the fast Fourier transform (FFT) size is 2048. Each radio frame is 10 ms long and consists of 10 subframes. In addition, normal cyclic prefix is assumed. Since we employ the per-RE uplink nulling, the self-interference channel estimation is done in a similar manner of conventional downlink channel estimation.

Experimental Results

We can see the effects of antenna separation and RF self-interference cancellation in Fig. 6b. The dual-polarized antenna can suppress the self-interference power about 17 dB. The RF self-interference cancellation circuit can further reduce the self-interference power by 6–8 dB with 1-tap RF cancellation and by 9–20 dB with 2-tap RF cancellation. We observe the frequency selectivity in the signal after RF cancellation, which can easily be handled with the per-subcarrier-based cancellation technique in a digital domain.

The effect of digital self-interference cancellation can be seen by comparing Fig. 6c (constellation before digital cancellation) and Fig. 6d (constellation after digital cancellation). The self-interference component is successfully cancelled by subtracting the a priori known transmitted signal using the self-interference channel estimate.

Conclusion

This article introduces the essential techniques to support LTE-compatible full-duplex radio. Our approach is based on a realistic LTE/LTE-A network model assuming full-duplex eNodeB and half-duplex UE. In order to support wideband and wide dynamic range RF self-interference cancellation, we develop a multi-tap, variable-gain, and self-adaptive RF self-interference cancellation circuit. For digital self-interference cancellation, we provide a new frame structure design that can perform accurate self-interference channel estimation with the use of uplink nulling schemes. The proposed techniques for LTE-compatible full-duplex radio were evaluated through system-level simulations and real-world testbed experiments. We can see that self-interference can be efficiently cancelled with a combination of RF and digital cancellation techniques.

The various techniques discussed in this article not only enable fast deployment of the full-duplex functionality over the existing LTE/LTE-A networks

and legacy UEs, but also provide a stepping stone to better develop further enhanced full-duplex techniques along with the development of 5G wireless networks.

References

[1] J. G. Andrews *et al.*, "What Will 5G Be?," *IEEE JSAC*, vol. 32, no. 6, June 2014, pp. 1065–82.

[2] D. Kim, H. Lee, and D. Hong, "A Survey of In-Band Full-Duplex Transmission: From the Perspective of PHY and MAC Layers," *IEEE Commun. Surveys & Tutorials*, vol. 17, no. 4, Nov. 2015, pp. 2017–46.

[3] K. S. Kim *et al.*, "16-QAM OFDM-Based W-Band Polarization-Division Duplex Communication System with Multi-Gigabit Performance," *ETRI J.*, vol. 36, no. 2, Apr. 2014, pp. 206–13.

[4] D. Bharadia, E. McMilin, and S. Katti, "Full Duplex Radios," *Proc. ACM SIGCOMM 2013*, Aug. 2013, pp. 375–86.

[5] T. Huusari *et al.*, "Wideband Self-Adaptive RF Cancellation Circuit for Full-Duplex Radio: Operating Principle and Measurements," *Proc. IEEE VTC-Spring 2015*, May 2015, pp. 1–7.

[6] S. Goyal *et al.*, "Full Duplex Cellular Systems: Will Doubling Interference Prevent Doubling Capacity," *IEEE Commun. Mag.*, vol. 53, no. 5, May 2015, pp. 121–27.

[7] 3GPP TS 25.104, "Base Station (BS) Radio Transmission and Reception (FDD)," v. 12.7.0, Jan. 2016; http://www.3gpp.org/DynaReport/25104.htm, accessed Oct. 31, 2016.

[8] M. Helno *et al.*, "Recent Advances in Antenna Design and Interference Cancellation Algorithms for In-Band Full Duplex Relays," *IEEE Commun. Mag.*, vol. 53, no. 5, May 2015, pp. 91–101.

[9] M. Chung *et al.*, "Prototyping Real-Time Full Duplex Radios," *IEEE Commun. Mag.*, vol. 53, no. 9, Sept. 2015, pp. 56–63.

[10] R. M. Vaghefi et al., "Cooperative Received Signal Strength-Based Sensor Localization with Unknown Transmit Powers," *IEEE Trans. Signal Processing*, vol. 61, no. 6, Mar. 2013, pp. 1389–1403.

[11] S. Kim *et al.*, "A 2.59-GHz RF Self-Interference Cancellation Circuit with Wide Dynamic Range for In-Band Full-Duplex Radio," *Proc. IEEE Int'l. Microwave Symp.*, May 2016.

[12] A. Sabharwal *et al.*, "In-Band Full-Duplex Wireless: Challenges and Opportunities," *IEEE JSAC*, vol. 32, no. 9, Sept. 2014, pp. 1637–52.

[13] 3GPP TR 36.913, "Requirements for Further Advancements for E-UTRA (LTE-Advanced)," v. 12.0.0, Oct. 2014; http://www.3gpp.org/DynaReport/36913.htm, accessed Oct. 31, 2016.

[14] T. Rappaport, *Wireless Communications: Principles and Practice*, 2nd ed., Prentice Hall, 2002.

[15] 3GPP TR 36.872, "Small Cell Enhancements for E-UTRA and E-UTRAN — Physical Layer Aspects," v. 12.0.0, Dec. 2013; http://www.3gpp.org/DynaReport/36872.htm, accessed Oct. 31, 2016.

Biographies

GOSAN NOH [S'07, M'12] (gsnoh@etri.re.kr) received his B.S. and Ph.D. degrees in electrical and electronic engineering from Yonsei University, Seoul, Korea, in 2007 and 2012, respectively. From March 2012 to February 2013, he was a postdoctoral researcher at the School of Electrical and Electronic Engineering, Yonsei University. Since March 2013, he has been with the Electronics and Telecommunications Research Institute (ETRI), Daejeon, Korea, where he is a senior researcher. His research interests include millimeter-wave transmission and high-speed train communications.

HANHO WANG joined the Information and Telecommunication Engineering Department of Sangmyung University in 2012, where he serves as an assistant professor. He received his B.S.E.E. ('04) and Ph.D. ('10) degrees from Yonsei University. He previously worked at the Korean Intellectual Property Office (KIPO) as a patent examiner in the Department of Information and Telecommunication Patent Examination.

CHANGYONG SHIN [S'04, M'07] received his B.S. ('93) and M.S. ('95) degrees from Yonsei University, Seoul, South Korea, and his Ph.D. ('06) degree from the University of Texas at Austin, all in electrical engineering. From 2007 to 2014, he was a principal research engineer with Samsung Advanced Institute of Technology, South Korea, where he worked on next-generation cellular systems. Since 2014, he has been with the School of Mechanical and ICT Convergence Engineering at Sun Moon University, South Korea.

SEUNGHYEON KIM received B.S. (2010) and Ph.D. (2016) degrees in electrical engineering from Kwangwoon University, Seoul, Korea. He is a staff engineer at GCT Semiconductor Inc., Seoul, Korea, where he is involved in wideband saw-less CMOS receiver design for LTE applications.

YOUNGIL JEON received his B.S. (2015) degree in electrical engineering from Kwangwoon University, where he is currently a Master's student. His research interests are in RF circuits and systems design for wireless communications.

HYUNCHOL SHIN [S'93, M'01, SM'10] joined the faculty of Kwangwoon University in 2003, where he is currently a professor. He received B.S. (1991), M.S.(1993), and Ph.D. (1998) degrees in electrical engineering from Korea Advanced Institute of Technology (KAIST), Daejeon, and held a postdoctoral position at the University of California Los Angeles (2003–2004). He has worked for several research companies, including Daimler-Benz Research Center, Samsung Electronics, and Qualcomm, as an RF/analog circuit designer for wireless communications. He has co-authored over 70 journal and conference papers, and holds over 30 patents. He has served on the Technical Program Committees of several IEEE conferences including ISSCC, VLSI Circuit Symposium, and A-SSCC.

JINUP KIM received his B.S. degree from Korea University, Seoul, Korea, in 1985, and M.S. and Ph.D. degrees from KAIST in 1987 and 1996, respectively. He has been with ETRI since 1987. He was a professor at the University of Science and Technology in the field of wireless communications during 2005–2010. He has researched in the field of wireless communication systems. He is currently interested in digital RF and software defined radio/cognitive radio technologies, and virtualization of the 5G access platform.

ILGYU KIM received B.S. and M.S. degree in electronic engineering from the University of Seoul, Korea, in 1993 and 1995, and his Ph.D. degree in information communications engineering from KAIST in 2009. Since 2000, he has been with ETRI, where he has been involved in the development of WCDMA, LTE, and MHN systems. Since 2012, he has been the leader of the mobile wireless backhaul research section. His main research interests include millimeter-wave communications and 5G mobile communications.

The various techniques discussed in this article not only enable fast deployment of the full-duplex functionality over the existing LTE/LTE-A networks and legacy UEs, but also provide a stepping stone to better develop further enhanced full-duplex techniques along with the development of 5G wireless networks.